On resistive interchange, double tearing, and resonant and non-resonant infernal modes in spherical tokamak negative central shear discharges

S.C. Jardin
Princeton Plasma Physics Laboratory, P.O.Box 451, Princeton, NJ 08543 USA
Corresponding author: jardin@pppl.gov

(Dated: July 10, 2025)

We examine the linear and nonlinear stability of a sequence of reversed shear NSTX equilibria with the same toroidal current density and pressure profile, but with different toroidal field strength. All equilibria have two $q = 2$ surfaces and have $q > 1$ everywhere. For this sequence, which all have $\beta_P \sim 0.5$, as the minimum value of q decreases below about 1.4, the localized resistive interchange criteria is strongly violated and the unstable mode with toroidal mode number $n = 1$ changes its dominant poloidal mode number m from a $(m, n) = (2, 1)$ double tearing mode to a non-resonant $(1, 1)$ infernal mode. This $(1, 1)$ mode nonlinearly flattens both the current density and the pressure near the magnetic axis. The nigher-n unstable modes are all resistive infernal modes localized around the surface where q has a minimum and the magnetic shear vanishes. They generally saturate nonlinearly at low amplitude, but can cause magnetic surface breakup near the axis.

I. INTRODUCTION

There remains considerable interest in tokamak discharges with a non-monotonic safety factor profile (negative central shear, or NCS) in both conventional tokamaks [1–5] and spherical tokamaks [6, 7]. This configuration has led to substantial improvements in energy confinement [1, 8] and to the formation of transport barriers [9–14] in most all devices in which it has been studied. NCS is considered an option for future fusion pilot and power plants based on the tokamak [15, 16].

Many of the NCS discharges exhibit MHD activity which can terminate the improved confinement regime, and in some cases can terminate the discharge. The nature of this MHD activity has been the subject of many studies involving advanced 3D nonlinear MHD simulation codes. They have identified localized resistive interchange modes [17, 18], double tearing modes [19–23] , and infernal modes [4, 18] as responsible for the MHD activity.

Localized resistive interchange modes [24] can be unstable for moderate pressure gradients in the reversed shear region [25], but calculations indicate that these have relatively small growth rates and are likely to nonlinearly saturate at low amplitude [17].

Double tearing modes (DTMs) were first identified theoretically using linear reduced MHD in cylindrical geometry at zero pressure [26]. This paper has been widely cited and extended, but even recent papers extending this to finite β and/or nonlinearly have predominantly been in cylindrical or slab geometry [27–31].

Using a more realistic, toroidal, geometry brings in essential elements such as poloidal mode coupling and β-stabilization [32]. There is computational [17, 18, 33] and experimental [28] evidence that β is stabilizing to the $(m, n) = (2, 1)$ DTM in toroidal geometry (but not in cylindrical geometry), Here, and throughout this paper, m is the poloidal mode number and n is the toroidal mode number.

There have recently been a number of papers [19, 20, 34, 35] describing 3D toroidal resistive MHD simulations of the $(2, 1)$ DTM. However, these papers have largely emphasized the effect of the separation of the two $q = 2$ crossing points and the shear at these points. They have not discussed the importance of q_{min} and the stability to the $(1, 1)$ non-resonant mode as is the subject of the present work.

Infernal modes can be unstable if there is a large enough pressure gradient near the reversal point, q_{min}, where the magnetic shear vanishes [4, 18]. These can be ideal MHD modes (unstable even with zero resistivity), but the growth rates and range of unstable configurations increases greatly when resistivity is taken into account [36]. The unstable eigenfunctions for the ideal and resistive infernal modes differ from those of the DTM. While the $(2, 1)$ DTM eigenmode typically occupies all the magnetic surfaces between the two $q = 2$ crossings, the ideal and resistive infernal modes tend to be more radially localized around the q_{min} surface and to have poloidal mode number $m \approx nq_{min}$.

A recent publication [18] examined the MHD stability of a particular NSTX [37] discharge with a non-monotonic q-profile. In the present paper we extend that analysis to a family of equilibria, each with two $q = 2$ surfaces, but with different values of q_{min}. We show that as q_{min} approaches unity from above, the n=1 mode changes from being dominantly a $(2, 1)$ DTM to becoming dominantly a non-resonant $(1, 1)$ mode. This mode, with a strong poloidal m=1 component, is capable of nonlinearly flattening the current and pressure near the magnetic axis.

The remainder of this paper is organized as follows: Section II describes how we generate the family of equilibria being studied and gives their linear stability properties. Section III describes nonlinear resistive MHD simulations for each of the family of five equilibria and how the nonlinear consequences of the instabilities changes dramatically when q_{min} falls below about 1.4. In Section IV

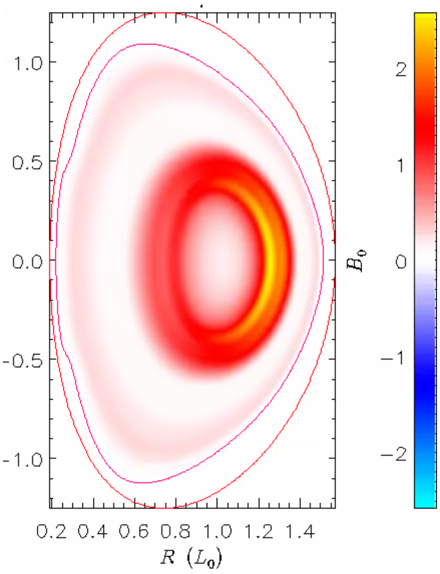

FIG. 1: Toroidal current density,$\mu_0 R J_\phi$ for the baseline equilibrium studied in Ref. [18]. Red curves show the computational boundary and the last closed flux surface.

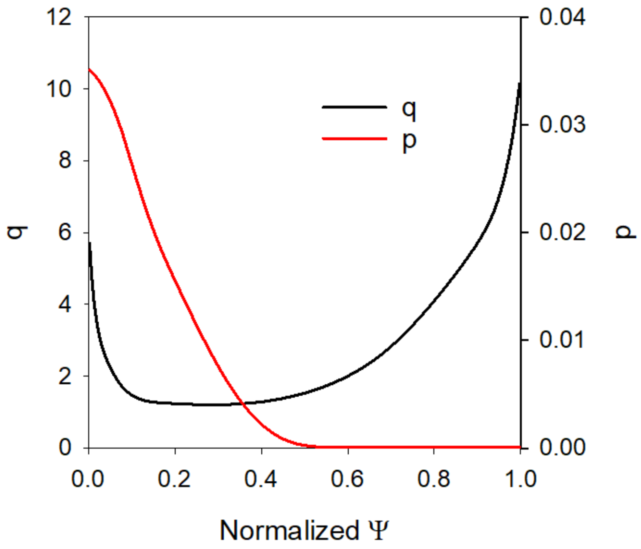

FIG. 2: Safety factor (q) profile and pressure profile ($\mu_0 p$) for the baseline equilibria studied in Ref. [18].

we apply a heating source to one of the "nonlinearly stable" equilibria and show that it remains stable even as β_P is doubled, although the surfaces become distorted. Section V presents a summary and discussion of some of the implications of this work.

II. EQUILIBRIUM AND LINEAR STABILITY

We start with the equilibrium studied in Ref. [18] and shown in Figs. 1 and 2. This was obtained from an EQDSK from NSTX shot 129169 at time 247 ms, just before a significant MHD event occurred in the discharge. (Note that the experimental uncertainty in q_{min} is difficult to quantify.)

We then generate a sequence of equilibria by applying different Bateman scaling factors [38], f_B, to this. The Bateman scaling leaves the pressure and toroidal current density unchanged, but increases the toroidal field at the boundary by a factor f_B, so that the safety factor (q-profile) changes. Shown in Fig. 3 are the q-profiles corresponding to f_B=1.4,1.2,1.0,0.95 and 0.90. (Note that f_B=1.0 is the original equilibrium.)

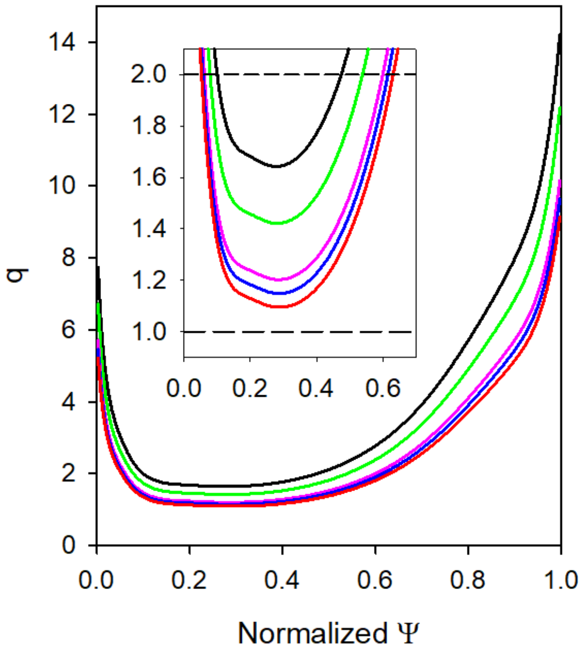

FIG. 3: Safety factor profiles for the present study obtained by applying a Bateman scaling factor (f_B) to the equilibrium used in Ref. [18]. From top to bottom, the curves correspond to f_B=1.40,1.20,1.00,0.95, and 0.90.

These equilibria all have poloidal beta $\beta_P \simeq 0.5$. This is a convenient way of generating a sequence of equilibria with the same poloidal beta and q-profile shape, but with differing values of q, in particular, different q_{min}. Figure 3 could be interpreted as a time sequence (top to bottom) of the current penetration phase of a NCS discharge with constant edge toroidal field but increasing toroidal current.

It is seen that all five equilibria have two $q = 2$ surfaces, and that as the scaling factor f_B decreases from 1.4 to 0.9, the minimum value of q , q_{min}, decreases, however $q_{min} > 1$ for all equilibria in the sequence.

The linear stability properties of these five equilibria, as computed with the linear version of the M3D-C^1 code [44], are summarized in Fig. 4 and in Table I. Shown in the figure are the ideal MHD (with zero resistivity) and the resistive MHD (with Spitzer resistivity) growth rates for the first 9 toroidal modes, $n = 1-9$, for each equilibria. Shown in the table, for each equilibrium, is the minimum value of the safety factor, q_{min}, and the dominant poloidal mode number, m, for each unstable mode with toroidal mode number n. In all cases, when both ideal and resistive modes are unstable, the m-number of both modes is the same.

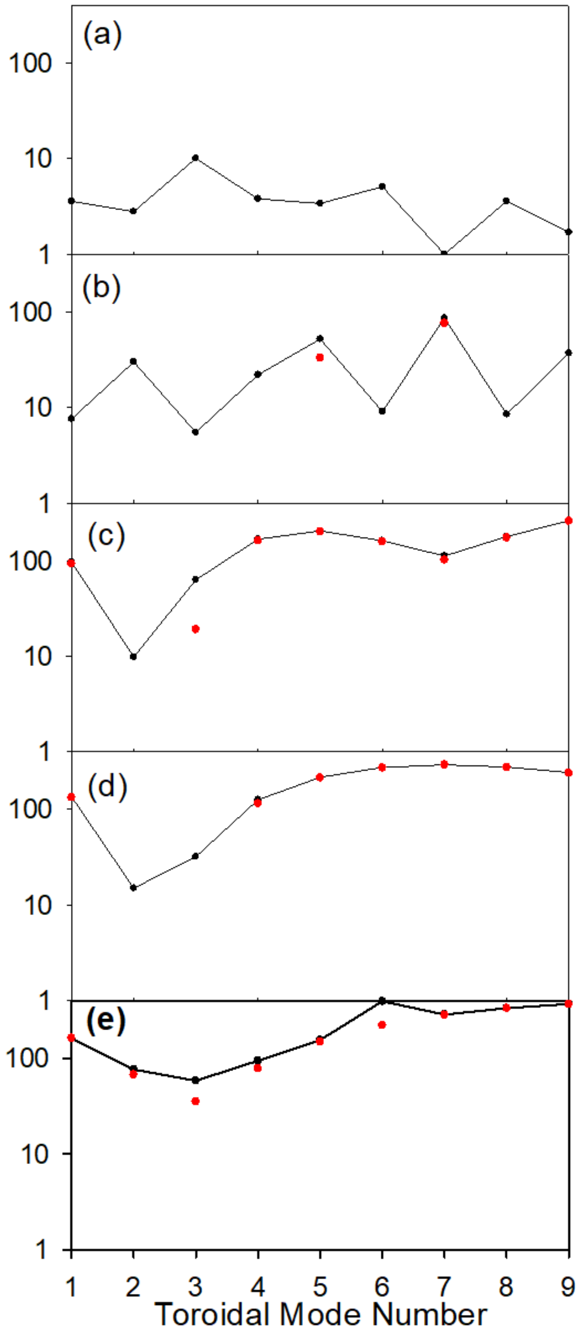

FIG. 4: Shown are the linear resistive (in black with connecting lines) and ideal (in red) growth rates, $\gamma\tau_A$, for each of the 9 toroidal modes ($n = 1-9$) for each of the five equilibria shown in Fig. 3, and in Table I: (a) $f_B = 1.4$, (b) f_B=1.2, (c) f_B=1.0, (d) f_B=0.95, and (e) f_B=0.90.

f_B	q_{min}	n=1	n=2	n=3	n=4	n=5	n=6	n=7	n=8	n=9
1.4	1.645	2	4	5	7	8	10	12	13	15
1.2	1.422	2	3	5	6	7	9	10	12	13
1.0	1.203	1	3	4	5	6	7	9	10	11
0.95	1.115	1	2	3	5	6	7	8	9	10
0.90	1.095	1	2	3	4	5	7	8	9	10

TABLE I: Minimum value of the safety factor, q_{min}, and the dominant poloidal mode number, m, for each of the 9 modes, $n = 1-9$, for each of the five equilibria shown in Fig. 3 whose growth rates are given in Fig. 4.

We note, from Fig 4, that the top equilibrium with f_B=1.4 and q_{min} = 1.645 is stable to all ideal MHD modes, whereas all the others are unstable to at least 2 ideal MHD modes. All the equilibria are unstable to resistive MHD modes for all n-numbers.

Consider the stability to the $n = 1$ mode as shown by the left-most symbols in each of the five graphs in Fig. 4. The top two equilibria, with f_B=1.4 and f_B=1.2, are stable in the ideal limit, whereas the bottom three entries are all unstable to ideal MHD n=1 modes. All equilibria are unstable to the $n = 1$ resistive mode with a growth rate that increases as the f_B factor decreases (q_{min} decreases towards 1).

But, we see from the column labeled $n = 1$ in Table I that there is also a significant change in the mode structure between the top two entries, f_B=1.4 and f_B=1.2, and the bottom three, $f_B \leq 1.0$. The poloidal mode structure changes from dominantly $m = 2$, as would be expected for a $(2, 1)$ DTM, to $m = 1$, a non-resonant $(1, 1)$ infernal mode. This is illustrated in Fig. 5 where we plot the linear eigenfunctions of the $n = 1$ resistive mode for each of the five equilibria. (We note here that Wesson [41] was likely the first to state that a $(1, 1)$ mode could be unstable if q had an off-axis minimum.)

It is also noted from Fig. 5 that in going from left to right, the radial extent of the mode shrinks from the entire region interior to the two $q = 2$ surfaces to a smaller volume, close to the q_{min} surface. This is a sign that the instability is shifting from being a classical $(2, 1)$ double tearing mode to a resistivity modified non-resonant $(1, 1)$ infernal mode [36, 39, 42, 43].

As a final observation from Table I, we note that only three resistive modes have the property that $m = 2n$ as would be the case for $q = 2$ double tearing modes. These are the $n = 1$ and $n = 2$ modes for f_B=1.4 and the $n = 1$ mode for f_B=1.2. For all the other modes the m/n resonant surface is either just above q_{min} for that equilibrium, or is non-resonant (slightly below q_{min} but above or equal to 1.0). These are all resistive infernal modes. The unstable eigenmodes for the basline equilibrium (with f_B=1.0) is given in Fig. 3 of Ref. [18]. The eigenmodes for the other equilibria are very similar, with well identified poloidal mode numbers and localized about the q_{min} surface.

We have also investigated these equilibria for stability to localized resistive interchange modes [24, 32] and the

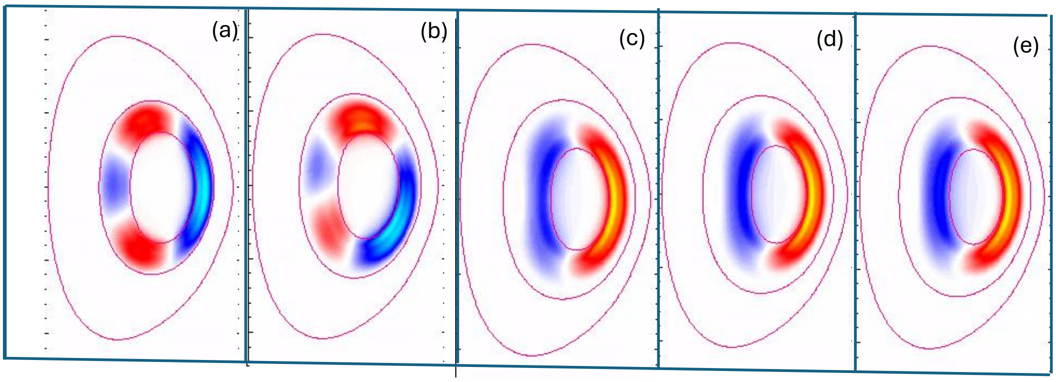

FIG. 5: Plotted are the perturbed pressure for the linearly unstable $n = 1$ resistive mode for each of the five equilibria listed in Table I and with q-profiles shown in Fig. 3. The three contour lines in eqch figure correspond to the last closed flux surface and the two $q = 2$ surfaces. Left to right, the equilibria correspond to (a) f_B=1.4, (b) f_B=1.2, (c) f_B=1.0, (d) f_B=0.95, and (e) f_B=0.90.

result is shown in Fig. 6. Shown is the surface-averaged quantity D_R as a function of the normalized poloidal flux ψ. (Only the inner 40% is shown as the outer surfaces are all stable. For more information on how D_R is computed, see Appendix C of Ref. [18].) A given surface is unstable to localized resistive interchange modes for $D_R > 0$. We see a large difference between the very unstable equilibria with f_B=0.9, 0.95, and 1.0, and the marginally unstable ones with f_B=1.2 and 1.4. This again shows that as q_{min} gets closer to 1.0 from above, the configuration becomes more unstable.

III. NONLINEAR EVOLUTION

We next consider the non-linear evolution of each of the five equilibria shown in Fig. 3 and listed in Table I. The EQDSK equilibrium, with the appropriate Bateman scaling factor, f_B, applied are loaded into the 3D nonlinear resistive MHD code M3D-C^1 [44] in which the following equations are evolved in time:

$$\frac{\partial n}{\partial t} + \nabla \cdot (n\mathbf{V}) = \nabla \cdot D\nabla n \tag{1}$$

$$\frac{\partial \mathbf{A}}{\partial t} = -\mathbf{E} - \nabla\Phi \tag{2}$$

$$\nabla_\perp \cdot \frac{1}{R^2}\nabla\Phi = -\nabla_\perp \cdot \frac{1}{R^2} \cdot \mathbf{E} \tag{3}$$

$$\mathbf{E} + \mathbf{V} \times \mathbf{B} = \eta\mathbf{J} - \lambda_H \Delta^* J_\phi \nabla\phi \tag{4}$$

$$nM_i\left(\frac{\partial \mathbf{V}}{\partial t} + \mathbf{V}\cdot\nabla\mathbf{V}\right) + \nabla p = \mathbf{J}\times\mathbf{B} - \nabla\cdot\Pi \tag{5}$$

$$\frac{3}{2}\left[\frac{\partial p}{\partial t} + \nabla\cdot(p\mathbf{V})\right] = -p\nabla\cdot\mathbf{V} + \mathbf{J}\cdot\mathbf{E} - \nabla\cdot\mathbf{q} + S_E \tag{6}$$

The magnetic field and current density are then determined by $\mathbf{B} = \nabla \times \mathbf{A}$ and $\mathbf{J} = \nabla \times \mathbf{B}$. The symbol $\nabla_\perp$ in Eq. (3) refers to the gradient in the (R, Z) plane in a (R, ϕ, Z) cylindrical coordinate system, and Δ^* is the standard toroidal elliptic operator that appears in the Grad-Shafranov equation. Equation (3) follows from the gauge condition on $\mathbf{A}$, $\nabla_\perp \cdot R^{-2}\mathbf{A} = 0$. The temperature is the pressure divided by the density, $T \sim p/n$. The linear form of the code used for linear stability studies is just the linearized form of these same equations.

The particle diffusion term D in Eq. (1) is a small

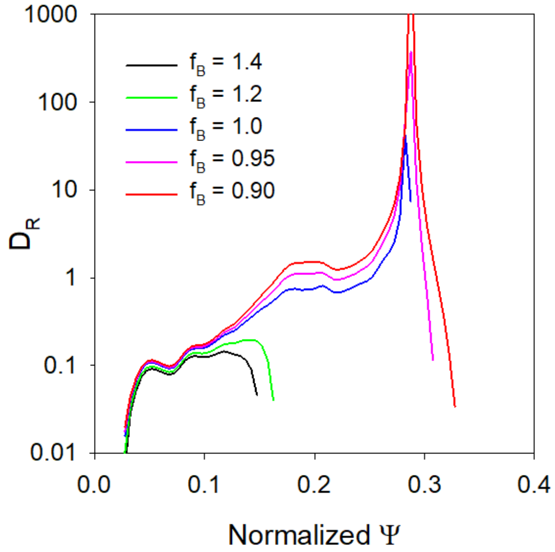

FIG. 6: Surface averaged resistive stability parameter D_R vs. normalized poloidal flux for the inner part of the equilibria. Curves from bottom to top correspond to f_B=1.4 (q_{min} = 1.645), f_B=1.2 (q_{min} = 1.422), f_B=1.0 (q_{min} = 1.203), f_B=0.95 (q_{min} = 1.115), and f_B=0.9 (q_{min} = 1.095). Equilibria become more unstable as q_{min} decreases towards 1.0.

term included to aid numerical stability. The resistivity η in Eq. (4) is the temperature-dependent Spitzer function [45]. The term involving λ_H is hyper-resistivity. A small value is used to improve numerical stability. The stress tensor in Eq. (5) is of standard form for viscosity [46], with viscosity coefficient μ. The heat flux vector, $\mathbf{q}$ in Eq. (6) has both an isotropic part and a part parallel to the magnetic field: $\mathbf{q} = -\kappa\nabla T - \kappa_{\|}\mathbf{bb}\cdot\nabla T$, where $\mathbf{b}$ is a unit vector in the direction of the magnetic field. The numerical values of the transport coefficients used in these calculations are given in Appendix A. The source term S_E given in Eq. (6) was zero for the calculations presented here in Section III but is used in Section IV as described in that section.

The M3D-C^1 code uses finite elements in all three dimensions. In the (R, Z) plane these are unstructured "Bell" triangular elements [47] that, for the baseline calculation, have a typical size of 1.2 cm. There were a total of 26130 vertices per plane. In these calculations we used 24 planes, with structured equally spaced Hermite cubic finite elements in the toroidal (ϕ) direction. As seen in Fig. 1, the computational grid extends slightly beyond the last closed flux surface (LCFS). The region between the LCFS and the computational boundary is treated as a high-resistivity low pressure plasma with electron temperature 25 eV. Conducting wall boundary conditions are imposed at the computational bounary.

The nonlinear calculations were initialized by giving the normalized velocities an incompressible random perturbation of order 10^{-8}. The time histories of the magnetic energy in each of the lowest 9 toroidal harmonics for each of the five nonlinear calculations are shown in Fig. 7.

Figure (7a) corresponds to f_B=1.4 which from Table I has $q_{min} = 1.645$. It is dominated by the $n = 9$ resistive infernal mode, which we see from Table I has the dominant poloidal mode number of 15. Thus, the resonant surface is at $q = 15/9 = 1.66$, very close to q_{min}. The $n = 9$ mode reaches a maximum and later decreases by an order of magnitude. The $n = 1$ mode, which we see from Fig. 5 and Table I is dominantly a $(2, 1)$ double tearing mode, never grows beyond $2. \times 10^{-7}$. There was very little change in the q-profile, and just a small change in the pressure profile, reducing the pressure gradient near the q_{min} surface. These changes are illustrated in Fig. 8 and in more detail in Fig. 9 (a) and (c).

It may seem surprising that the n=9 mode is dominant in the nonlinear run presented in Fig. (7a) and yet Fig. (4a) shows that the n=3 mode has the largest linear growth rate. For very short times, (the first 20 τ_A), the n=3 mode indeed grows up the fastest. However, there are so many unstable modes at the sam physical location that they all interfere with one another, and then eventually, after about 150 τ_A, the n=9 mode grows up out of the noise and dominates.

The f_B=1.2 nonlinear simulation, starting from the equilibrium with $q_{min} = 1.422$, is shown in Fig. (7b). It is very similar to the f_B=1.4 result. It is dominated by a $(m, n) = (13, 9)$ resistive infernal mode which has a resonant surface at $q = 13/9 = 1.444$, also very close to q_{min} for this equilibrium. The $n = 1$ harmonic, which is a $(2, 1)$ DTM, also remains small. (Further calculation shows that it saturates at about $1. \times 10^{-6}$ at t = 3500 τ_A.)

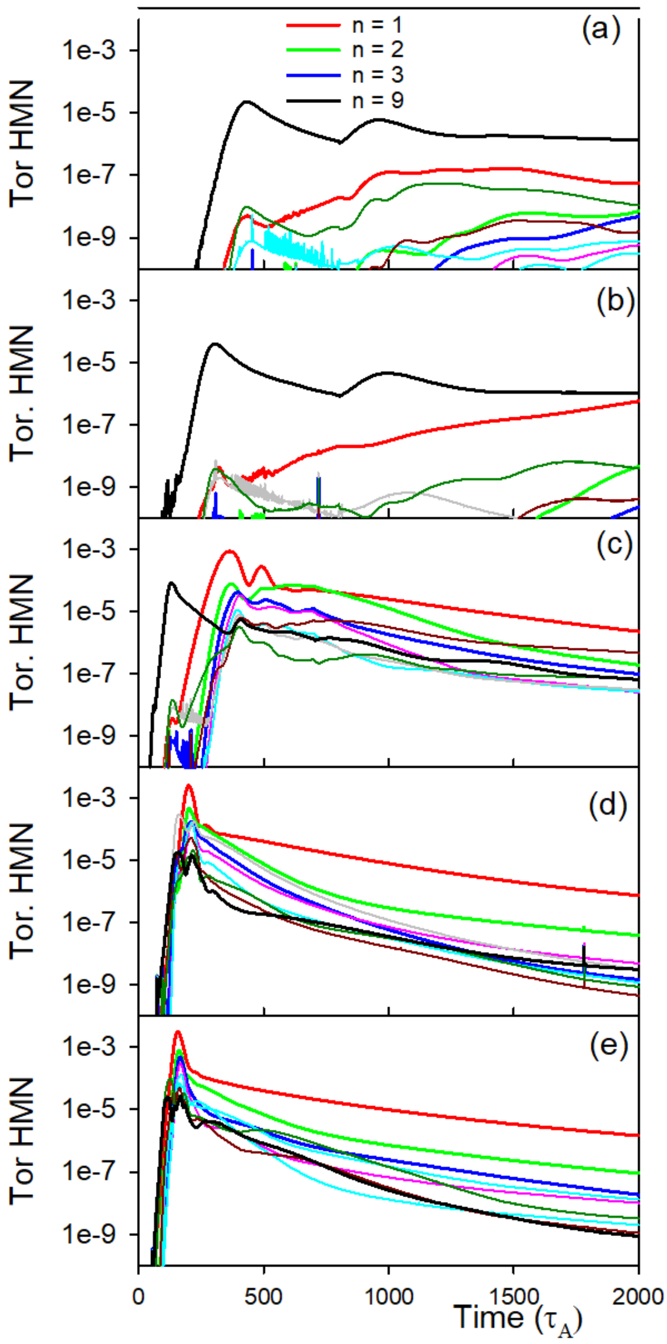

FIG. 7: Magnetic energy in each of the toroidal harmonics, for $n = 1 - 9$, for the nonlinear MHD calculations starting with each of the five equilibria shown in Fig. 3 and listed in Table I. The Bateman scaling factors ,f_B, for the five calculations are (a) $f_B = 1.4$, (b) f_B=1.2, (c) f_B=1.0, (d) f_B=0.95, and (e) f_B=0.90.

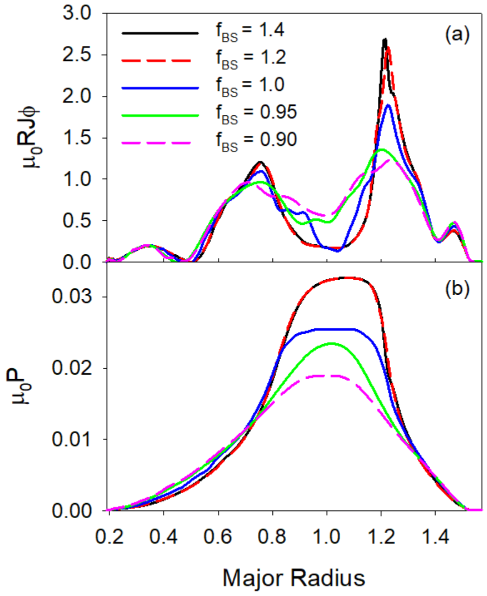

FIG. 8: Plotted are the midplane profiles at the toroidal plane $\phi = 0$ of (a) the toroidal current density and (b) the pressure at the end of each of the five calculations shown in Fig. 7.

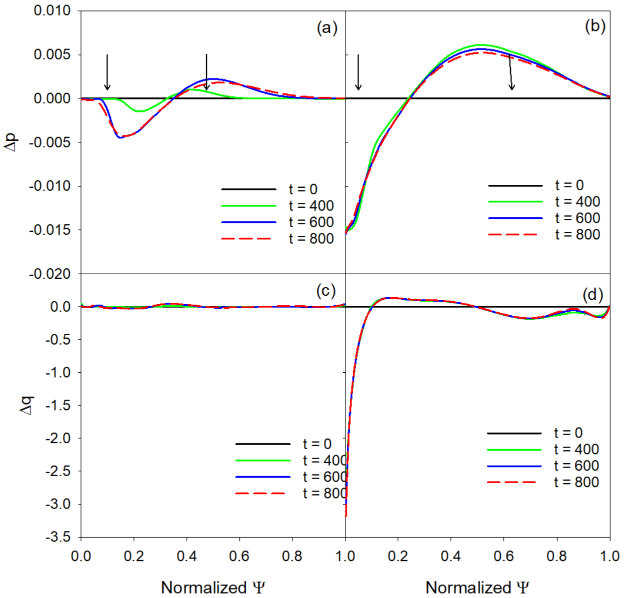

FIG. 9: Plotted in (a) and (b) are the changes (from time t=0) in the pressure profile and in (c) and (d) the changes in the q-profile at 4 times in the first and last nonlinear calculation shown in Fig. 3. i.e. (a) and (c) correspond to the f_B=1.4 calculation, and (b) and (d) to the f_B=0.9 calculation.

However, the picture changes dramatically for the bottom three plots of Fig. 7 corresponding to f_B=1.0 (c), f_B= 0.95 (d) and f_B=0.90 (e). Each of these has an unstable $(1, 1)$ ideal MHD mode which dominates the nonlinear evolution. The growth rate and maximum amplitude of the mode increase as f_B (and q_{min}) decrease. This mode is significant as it is the only mode with a significant $m = 1$ poloidal component that can extend to the magnetic axis and modify the current density, safety factor and pressure there.

Figure 8 shows midplane profiles of the final current density and pressure for each of the five calculations shown in Fig. 7. The curves for the first two calculations, with $f_B = 1.4$ and 1.2, almost overlay in both 8 (a) and (b) and are very little changed from those at time t=0. However, for $f_B = 1.0$, it is seen that the central current density starts to fill in and the central pressure is reduced. The central current density fill in and the central pressure reduction is even greater for the curves coresponding to $f_B = 0.95$ and 0.90 which also had the largest $(1, 1)$ mode activity.

To further illustrate the differences between the highest and lowese q_{min} cases, we plot in Fig. 9 a comparison of the changes in the profiles for the top and bottom calculations shown in Fig. 7, corresponding to f_B=1.4 and f_B=0.9. Figure 9 (a) and (b) shows the changes in the pressure profiles for the f_B=1.4 and f_B=0.9 calculations at 4 times. (Note that to isolate the changes due to the instabilities, we actually are plotting Δp, the *difference* between the 3D result and that of a companion 2D result with the same transport coefficients.) The leftmost plot, (a), shows just a small, localized change in the pressure profile that reduced the pressure gradient near the q_{min} surface. (The two arrows indicate the initial q=2 surfaces.) There is essentially no change in Δp at the magnetic axis.

In contrast, Fig. (9b) shows a large redistribution of the pressure, with the largest decrease occurring at the magnetic axis. This is the result of the $(1, 1)$ mode as the poloidal m=1 mode nonlinearly extends to the magnetic axis.

The comparison of the changes in the two q-profiles, as shown in Figs. 9 (c) and (d) is even more dramatic. The f_B=1.4 calculation shown in (c) has almost no change in q, whereas the f_B=0.9 calculation shown in (d) has a large change in q at and near the axis, essentially filling in the current near the axis so that the configuration is no longer NCS.

IV. STABILITY AT HIGHER β_P

We saw from Fig. (7a) that the configuration with f_B=1.4 (q_{min} = 1.645) was non-linearly stable with β_P = 0.5 (as was the case with f_B=1.2). We next explore if the configuration remains stable at higher β_P.

Figures 10-12 summarize a calculation in which the calculation shown in Fig. (7a) is extended to time 5200 τ_A, but with a heatng source added at time t = 2000 τ_A (and then removed at t = 4000 τ_A) so that the β_p doubles, from 0.5 to 1.0 in the time interval t=2000 τ_A - 4000 τ_A and then stays fixed as shown in Fig. (10a). The

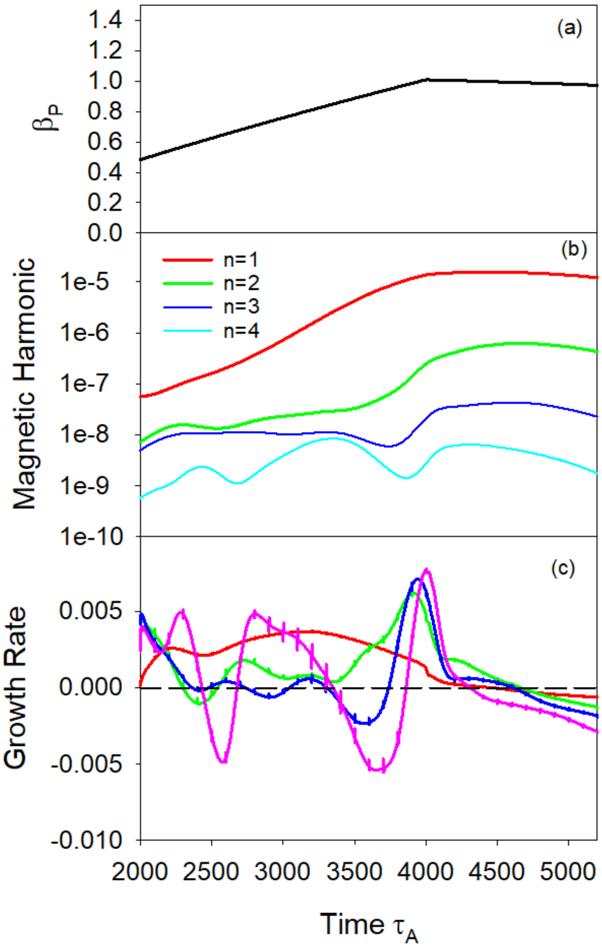

FIG. 10: The calculation shown in Fig. (7a) is extended for an additional 3200 τ_A with a heating source applied at time t = 2000 τ_A and then removed at time t = 4000 τ_A. (a) β_P vs time; (b) magnetic energy in the first 4 toroidal harmonics vs time; (c) growth rates of the first 4 toroidal harmonics vs time.

heating source had spatial dependence $S_E \sim exp(-((R-R_0)^2+(Z-Z_0)^2)/\delta^2)$ where $R_0 = 1.0$ m, $Z_0 = 0.0$, and $\delta = 0.4$ m.

We see from Fig. (10b) that the magnetic energy in the $n = 1$ harmonic in particular increases as the β_P increases, but levels off once β_P stops increasing. We see from Fig. (10c) that at the end of the calculation, the growth rates for all modes, n=1-4, are negative, indicating MHD stability at that higher β_P value. (Modes with $n > 4$ were included in the calculation but had very small amplitudes and are not included in the plot for clarity.)

Figure 11 (a) and (b) show contours of the toroidal current density at the start and the end of the calculation shown in Fig. 10. It is evident that the current density has changed very little, and that it remains hollow. Frames (c) and (d) show Poincaré plots at the start and finish of the calculation. While the surfaces look very good at the start (t = 2000 τ_A) , there are islands at the final time, and the surfaces closest to the original magnetic axis appear to be destroyed. This destruction of the innermost surfaces is likely due to the excitation of infernal modes centered at the surface where the minimum of q occurs, similar to what was seen in Ref. [42].

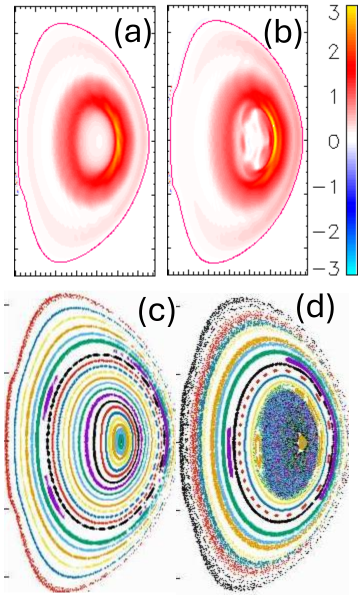

FIG. 11: Shown in (a) and (b) are the initial (t = 2000 τ_A) and final (t = 5200 τ_A) contours of the toroidal current density $\mu_0 RJ\phi$ at one toroidal plane for the calculation shown in Fig. 10. Shown in (c) and (d) are the Poincaré plots at these same two times.

Figure 12 shows the surface averaged pressure profile at three times for the calculation in Fig. (7a) and extended as shown in Fig. 10. The initial pressure (at time t=0) was taken from the Bateman scalled EQDSK as described in Section II. It changes in time due to diffusion, heating, and non-axisymmetric MHD activity. Also shown in the figure, in dashed lines are the profiles at the same times for a 2D calculation with the same transport coefficients and heating source. The difference between the 3D and the 2D curves is due to the effects if the non-axisymmetric MHD activity.

V. SUMMARY AND DISCUSSION

We generated a family of five equilibria from the experimentally obtained EQDSK reversed shear equilibrium studied in Ref. [18] by applying a Bateman scaling factor, f_B. These all have the same q-profile shape, but have q_{min} ranging from 1.095 to 1.645. These are all linearly unstable to resistive modes with toroidal mode number n=1-9 and beyond.

The modes with toroidal mode number $n > 2$ are all resistive infernal modes with $m/n \simeq q_{min}$, and are highly localized around the q_{min} surface. The unstable n=1 mode for the equilibria with the highest q_{min} val-

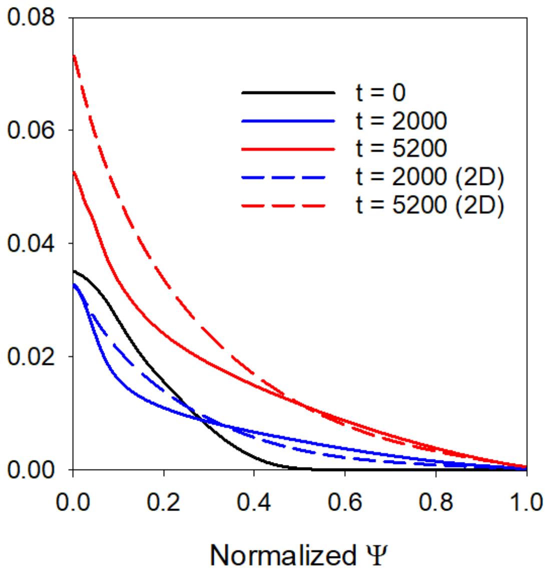

FIG. 12: Surface averaged pressure profile vs normalized poloidal flux at three times for the calculations shown in Fig. (7a) continued with heating applied in Fig. 11. Also shown, in dashed lines, are the results of a 2D (axisymmetric) calculation witht he same transport coefficients and heating source at those same times.

ues, 1.645 and 1.422, are classical $(2, 1)$ DTMs, where the perturbation fills the region between the two $q = 2$ surfaces. However, the n=1 perturbations of the equilibria with lower q_{min}, 1.203, 1.115, and 1.095, are not DTMs, but are non-resonant $(1, 1)$ infernal modes. These three lower q_{min} equilibria also strongly violate the localized resistive interchange criteria.

Nonlinearly, we see a big difference between the two classes of equilibria. The higher q_{min} cases with the $(2, 1)$ DTMs saturate at a low amplitude and do not substantially modify the pressure or current density outside the two q=2 surfaces, including the region near the magnetic axis. The lower q_{min} cases with the unstable non-resonant $(1, 1)$ infernal modes, experience an internal reconnection event which largely fills in the initially hollow current profiles.

It is interesting that the experimentally realized equilibrium, which corresponds to $f_B = 1.0$ (the center frame of Fig. 7) is at or near the dividing line between these two classes of equilibria. As discussed in [18], a MHD event occurred in the discharge just after the time this equilibrium was reconstructed. Experimental reconstructions indicate that the q_{min} was falling and the central pressure was increasing just before the MHD event occurred.

A follow-on calculation applied a heating source to the non-linearly saturated high-q_{min} case and doubled the β_P. The configuration non-linearly reached a new stable state but with some degredation in the quality of the magnetic surfaces, especially near the original magnetic axis.

This study highlights the importance of the value of q_{min} in NCS discharges. If q_{min} can be kept above approximately 1.3 or 1.4, perhaps by current drive, it may be possible to maintain the NCS configuration indefinitely, although it is not clear if the favorable transport properties of this configuration would survive if the magnetic surfaces begin to break up.

Finally, we note that the work presented here made use of a resistive MHD model neglecting equilibrium flow. Other effects such as plasma diamagnetic flows [48], particle trapping, and other intrinsically kinetic effects could affect the results given here but are outside the scope of this study.

VI. ACKNOWLEDGEMENTS

This work was supported by the U.S. DoE Award No. DE-AC02-09CH11466. The calculations were performed on the Perlmutter supercomputer at the National Energy Research Supercomper Center (NERSC), and on the stellar computer at Princeton University. The author acknowledges essential software support from J. Chen and the SCOREC team at RPI.

VII. DATA AVAILABILITY

The data that supports the findings of this study are available upon reasonable request.

Appendix A: Transport Coefficients

In Table II we list the numerical values of the normalized and actual transport coefficients appearing in Eq. 1-6 that were used in the nonlinear calculations presented in Sec. III and IV. The resistivity used was the Spitzer resistivity [45]. The initial central value of the plasma density was $n(0) = 2 \times 10^{19} m^{-3}$ and the initial central electron temperature was $Te(0) = 2.8 KeV$.

variable	M3D-C^1	dimensionless value	SI value
D	denm	$1. \times 10^{-6}$	$2.18 m^2 s^{-1}$
κ	kappat	$1. \times 10^{-6}$	$2.18 \times 10^{20} m^{-1} s^{-1}$
$\kappa_{\|\|}$	kappar	1.0	$2.18 \times 10^{26} m^{-1} s^{-1}$
λ_H	hyper	1.25×10^{-10}	$3.7 \times 10^{-20} m^2 s$
$\eta(0)$	eta	4.3×10^{-9}	$1.3 \times 10^{-18} s$
μ	amu	$1. \times 10^{-5}$	$43.65 \times 10^{-6} Pa \cdot s$

TABLE II: Transport coefficients for the nonlinear calculation of Sec. III . Listed are the initial central values of the resistivity, η, , which is a function of space and time, and the initial value of the viscosity, μ which changes in time as described in the text.

All nonlinear calculations used a constant time step of dt = 1.0 (dimensionless) = $0.46 \mu s$ (SI). In all calculations the viscosity began at $\mu = 1. \times 10^{-5}$ but was increased during the calculation if and when numerical instabilities started to grow and cause the calculation to crash. For f_B=1.4, μ was increased to $8. \times 10^{-5}$ at t=800. For f_B=1.2, μ was increased to $5. \times 10^{-5}$ at t=800. For f_B=1.0,, μ was increased to $5. \times 10^{-5}$ at t=700, and then $8. \times 10^{-5}$ at t=800. For f_B=0.95, μ was increased to $5. \times 10^{-5}$ at t=200. For f_B=0.90, μ was increased to $5. \times 10^{-5}$ at t=100, and then to $8. \times 10^{-5}$ at t=500. It is our experience that changing the viscosity in this range does not change the qualitative stability properties, but rather only affects the instantaneous growth rates.

ORCID IDs

S.C.Jardin 0000-0001-6390-6908

end

---

[1] Levinton, F.M., Zarnstorff, M.C., Batha, S..H., Bell,M., Bell, R.E, Budny, R.V., Bush, C., Chang,Z., Fredrickson,E., Janos, A. *et al* "Improved Confinement with Reversed Magnetic Shear in TFTR", Phys. Rev. Lett. **74** 4416-4420 (1995)

[2] Strait, E. J., Casper, T. A., Chu, M.S., Ferron, J.R., Garofalo, A., Greenfield, C. M., LaHaye, R. J.,Lao, L.L. Lazarus, E.A., Miller, R.L., *et al*, "Stability of negative central magnetic shear discharges in the DIII-D tokamak", Phys. Plasmas **4**, 1783-1791 (1997)

[3] Maget, P., Huysmans, G., Garbet, X., Ottaviani, M., Lutjens, H., Luciani, J. F., "Nonlinear MHD simulation of the tore supra hollow current curent profiles discharge", Phys. Plasma, bf 14, 052509 (2007)

[4] Bierwage, A., Toma, M., Shinohara, "MHD and resonant instabilities in JT-60SA during current ramp-up with off-axis N-NB Injection", Plasma Phys. Control. Fusion, **59**, 125008 (2017)

[5] Reisner, M., DiSiena, A., Fable, E., Stober, J., Fischer, R., McDermott, R.M., Bilato, R., Bock, A., Gorler, T., and the ASDEX Upgrade Team, "Parametric dependencies of ion temperature profile peaking in ASDEX Upgrade high-beta scenarios", Nucl. Fusion **65**, 016024 (2025)

[6] Berkery, J. W., Sabbagh, S. A., Kogan, L., Gibson, S., Ryan, Zamkovska, V., Butt, J., Harrison, J., Henderson, S., and the MAST-U team, "Operational space and performance limiting events in the first physics campaign of MAST-U", Plasma Phys. Control. Fusion **65** 045001 (2023)

[7] Uzun-Kaymak, U, Foley, E.L., Calante, M.E., and Levinton, F.M., "Forming a database to study reversed magnetic shear from the National Spherical Torus eXperiment using machine learning", Phys. Plasmas **31**, 112506 (2024)

[8] Yuh, H. Y., Kaye, S.M., Levinton, F. M., Mazzucato, E., Mikkelson, D. R., Smith, D. R., Bell, R. E., Hosea, J. C., LeBlanc, B.,P., Peterson, J. L., *et al* "Suppression of Electron Temperature Gradient Turbulence via Negative Magnetic Shear in NSTX", Phys. Rev. Lett., **106**, 055003 (2011)

[9] Yuh, H. Y., Levinton,F. M., Bell, R. E., Hosea, J. C., Kaye, S. M., LeBlanc, B. P., Mazzucaro, E., Peterson, J. L., Smith, D. R., Candy, J., *et al*, “Internal Transport Barriers in NSTX”, Phys. Plasmas **16**, 056120 (2009)

[10] Sakamoto, Y., Suzuki, T., Ide, S.,Koide, Y., Takenaga, H., Kamada, Y., Fujita, T., Fukuda, T., Takizuka, T., Shirai, H., *et al* "Proprties of internal transport barrier formation in JT-60U", Nucl. Fusion **44** 876 (2004)

[11] Conway, G.D., Peeters, A.G., Gruber, O., Gude, A., Gunter,S., Kurzan, B., Maraschek, M., Meister, H., Muller, H.W. *et al* "Turbulence reduction in internal transport barriers on ASDEX Upgrade" Plasma Physi. Control. Fusion *43* 1239 (2001)

[12] Dux, R., Giroud, C., Zastrow, K.-D., and JET EFDA contributors, "Impurity transport in internal transport barrier discharges on JET", Nucl. Ffusion **44**260 (2004)

[13] Chung J., Hahn, S.H., Han, H., Kang, J., Kim, H.S., Jeon, Y.M., Ko, J., Lee, K. D., Ko, W.H. ,Seo, S.H., *et al* "Sustainable internal transport barrier discharge at KSTAR" Nucl. Fusion **61** 126051 (2021)

[14] Wu, M., Liu, Z., Li, G., Han, X., Zhang,T., Li, Y., Zhou, T., Chao, Y., Wang, S., Wu, X., *et al* Experimental study of the core instability before and after intrnal transport barrier formation in EASE", Nucl. Fusion, **63** 016008 (2023)

[15] Buttery, R.J., Park, J.M., McClenaghan, J.T., Weisberg, D., Ferron, J., Garofalo, A., Holcomb, C.G., Leuer, J.,Snyder, P.B., "The advanced tokamak path to a compact net electric fusion pilot pland", Nucl. Fusion, **61** 046028 (2021)

[16] Menard, J.E., Grierson, B.A., Brown, T., Rana, C., Zhai, Y., Poli, F.M., Maingi, R., Guttenfelder, W., Snyder, P.B., "Fusion pilot plant performance and the role of a sustained high power density tokamak", Nucl. Fusion **62** 036026 (2022)

[17] Leboeuf, J. N., Lynch, V. E., and Carreras, B. A., “Linear and nonlinear resistive magnetohydrodynamic stability of tokamak discharges with negative central shear" Phys. Plasmas **8**, 3358-3366 (2001)

[18] Jardin, S.C., Munaretto, S., Ferraro, N. M., Kaye, S. M., Kleiner, A., and Lyons, B.C., "MHD stability of spherical tokamak equilibria with non-monotonic q-profiles", Phys. Plasmas **31**, 032503 (2024)

[19] Zhang, W., Ma, Z., Zhu, J., Zhang, W.W., "Core-crash sawtooth associated with $m/n = 2/1$ double tearing modes in Tokamaks", Plasma. Physics Control. Fusion, **61**, 075002 (2019)

[20] Zhang,W., Lin, X., Ma, Z. W. ,Lu, X. Q,, and Zhang, H. W., "The off-axis pressure crash associated with the nonlinear evolution of the m/n = 2/1 double tearing mode", Phys. Plasmas **27** . 122509 (2020)

[21] Nardon, E., Bandaru, V., Hoelzl, M., Artola, F. J., Maget, P., "Non-linear dynamics of the double tearing mode", Phys. Plasmas **30**, 092502 (2023)

[22] Maget, P., Lutjens, H., Coelho, R., Alper, B., Brix, M., Burattr, P., Buttery, R. J., DelaLuna, E., Hawkes, N., Huysmans, G., Jenkins, I., Challis, C.D., Giroud, C., Litaudon, X., Mailloux, J. Ottaviani, M., "Modelling of (2,1) NTM threshold in JET advanced scenarios", Nucl. Fusion **50** 045004 (2010)

[23] Maget, P., Lutjens, H., Luciani, J. F., Garbet, X., Fevrier, O., Segui, J.L., "Bi-fluid and neoclassical effect of a double-tearing mode in Tore Supra", Phys Plasmas

bf 21, 062504 (2014)

[24] Glasser, A. H., Greene, J. M., and Johnson, J. L., ”Resistive instabilities in general toroidal plasma configurations”, Physics of Fluids, **18**, p. 875 (1975)

[25] Chu, M.S., Greene, J.M., Lao, L.L., Miller, R.L, Bondeson, A., sauter, O, Strait, E.I., Taylor, T.S., and Turnbull, A.D., ”Resistive Interchange Modes in Negative Central Shear Tokamaks with Peaked Pressure Profiles”, Phys. Rev. Lett, **13**, p 2710 (1996)

[26] Pritchett, P. L., Lee, Y. C., and Drake, J. F., “Linear analysis of the double tearing mode”, Physics of Fluids **23**, 1368-1374 (1980)

[27] zhang, D., Wu, Z., Ma, J., Guo,W., Huang, Y., Liu, H., ”Effect of plasma beta on the nonlinear evolution of m/n = 2/1 double tearing mode in high Lundquist number regime”,Nucl. Fusion **65** 026043 (2025)

[28] Gunter, S., Schade, S., Maraschek, M., Pinches, S.D., Strumberger, E., Wold, R., Yu, Q., ”MHD phenomena in reversed shear discharges on ASDEX Upgrade”, Nucl. Fusion **40** 1541 (2000)

[29] Yu, Q., Gunter, S., ”Fast magnetic reconnection and driven plasma rotation in reversed central magnetic shear configuration”, Nucl. Fusion **62** 126056 (2022)

[30] Ishii, Y., Azumi, M., Kishimoto, Y., ”Structure-driven nonlinear instability of double tearing mode and the abrupt growth after long-time-scale evolution”, Phys. Rev. Lett. **89** , 205002 (2002)

[31] Janvier, M, Kishimoto, U., Li, J. Q., ”Structure-driven nonlinear instability as the origin of the explosive reconnedtion dynamics in resistive double tearing modes”, Phys. Rev. Lett. **107**, 19500 (2011)

[32] Glasser, A.H., Greene, J. M., Johnson, J.L., ”Resistive Instabilities in a Tokamak”, Phys. Fluids **19** ,567-574 (1976)

[33] Wang, H., Wang, Z-X., Liu, T., Zhu, X.L., ”Effects of Plasma Boundary Shape on Explosive Bursts Triggered by Tearing Mode in Toroidal Tokamak Plasmas with Reversed Magnetic Shear”, Chinese Physic Letters, bf 40, 075201 (2023)+

[34] Li, J.Y., Liu, Z.X., Zhang, W., Ma, Z.W., Gao, X., Li, G.Q., Liu, H.Q., Wu, M.F., Liu, Y.J., Deng, C.C., *et al*, ”Numerical investigation of the 2/1 double tearing mode in EAST with the CLT code”, AIP Advances **13**, 105214 (2023)

[35] Zhang, W., Ma, Z., Zhang, H., Wang, X., ”Sawtooth-like oscillations and steady states caused by the m/n=2/1 double tearing mode”, Plasma Sci. Technol. **24** 035104 (2022)

[36] Charlton, L.A., Hastie, R. J., Hender, T.C., ”Resistive infernal modes”, Phys. Fluids B **1** 798-803 (1989)

[37] Ono, M., Kaye, S. M., Peng, Y.-K. M., Barnes, G., Blanchard, W., Carter, M.D., Chrzanowski, J., Dudek, l, Ewig, R.,Gates, D., *et al.*, ”Exploration of spherical torus physics in the NSTX device”, Nucl. Fusion **40**, 557 (2000)

[38] Bateman, G. and Peng, M., ”MHD Stability of Flux-Conserving Tokamak Equilibria”, Phys. Rev. Lett**38** 829 (1977)

[39] Manickam, J., Pomphrey, N., Todd, A., ”Ideal MHD stability properties of pressure driven modes in low shear tokamaks”, Nucl. Fusion **27**. 1461 (1987)

[40] Jardin, S.C., Ferraro, N., Breslau, J., and Chen, J., ”Multiple timescale calculations of sawteeth and other global macroscopic dynamics of tokamak plasmas”, Comput. Sci. & Disc., **5**, 014002 (2012)

[41] Wesson J., ”Sawtooth Oscillations”, Plasma Physics and Controlled Fusion, **28** 243 (1986)

[42] Jardin, S. C., Ferraro, N. M., Guttenfelder, W., Kaye, S. M. , Munaretto, S., ”Ideal MHD Limited Electron Temperature in Spherical Tokamaks Phys. Rev. Lett. **128** 245001 (2022)

[43] Jardin, S. C., Ferraro, N. M., Guttenfelder, W., Kaye, S. M. , Munaretto, S., ”Ideal MHD induced temperature flattening in spherical tokamaks”, Phys. Plasmas **128** 042507 (2023)

[44] Jardin, S.C., Ferraro, N., Breslau, J., and Chen, J., ”Multiple timescale calculations of sawteeth and other global macroscopic dynamics of tokamak plasmas”, Comput. Sci. & Disc., **5**, 014002 (2012)

[45] Huba, J.D., ”NRL Plasma Formulalry, Revised 2013”

[46] Landau, Lev, D, and Lifschitz,E. M., *Fluid Mechanics*, Vol. 6 (1st ed.) Pergamon Press (1959)

[47] Jardin, S., ”A triangular finite element with first-derivative continuity applied to fusion MHD applicaitons”, J. Comput. Phys. **200** pp. 133-152 (2004)

[48] brunetti, D., Graves, J. P., Halpern, F.D., Luciani, J.F., Lutjens, H., and Cooper, W.A., ”Extended MD simulations of infernal mode dynamics and coupling to tearing modes”, Plasma Physics and Controlled Fusion, **57** 054002 (2015)